International Journal of Biological Macromolecules 294 (2025) 139427

Contents lists available at ScienceDirect

International Journal of Biological Macromolecules

journal homepage: www.elsevier.com/locate/ijbiomac

DOPAC as a modulator of α-Synuclein and E46K interactions with membrane: Insights into binding dynamics

Elena Rizzotto [a,1], Andrea Pierangelini [a,1], Benedetta Fongaro [a], Manuela Leri [b], Ilenia Inciardi [a], Philipp Trolese [a], Vincenzo De Filippis [a], Monica Bucciantini [b], Laura Acquasaliente [a,*], Patrizia Polverino de Laureto [a,*]

[a] Department of Pharmaceutical and Pharmacological Sciences, University of Padova, Padova, Italy
[b] Department of Biomedical, Experimental and Clinical Sciences Mario Serio, University of Firenze, Firenze, Italy

ARTICLE INFO

Keywords:
α-Synuclein
E46K familiar mutation
Membrane binding properties
DOPAC
Conformational studies

ABSTRACT

α-Synuclein (Syn) is an intrinsically disordered protein, abundant in presynaptic neurons. It is a constituent of the Lewis Body inclusions as amyloid fibrils, in Parkinson's disease patients. It populates an ensemble of conformations and floats between the free random coil and the membrane-bound α-helical species. E46K is a pathogenic mutant of Syn able to accelerate the formation of fibrils. The lysine in position 46 affects several protein structural properties including its interaction with membranes.

We have shown that 3,4-dihydroxyphenylacetic acid (DOPAC), a dopamine metabolite, hampers Syn to form fibrils, interfering with the aggregation process and alters the interaction of the protein and its aggregates with membranes. To understand the mechanism of such alteration, we studied the interplay between Syn and E46K, lipid membranes and DOPAC. The ability of DOPAC to displace the proteins bound to membrane was also tested.

Our findings provided a dynamic model of interaction able to explain the different effects of DOPAC on lipid binding properties of Syn and E46K, shedding light on the conformational changes induced by the catechol, which may destabilize the protein interactions with membranes. Understanding these mechanisms could have implications for therapeutic strategies targeting Syn aggregation and membrane interactions in neurodegenerative diseases.

1. Introduction

Parkinson's disease (PD) is a chronic, progressive neurodegenerative disease mainly characterized by motor symptoms [1]. Its neuropathological hallmarks are the loss of dopaminergic neurons in the substantia nigra, with dopamine deficiency, and widespread intracellular inclusions, called Lewy bodies, containing aggregates of the protein α-synuclein (Syn) [2]. Syn is a relatively small protein (14.460 Da), prevalently present in the presynaptic nerve terminals (Fig. 1A). In vivo and isolated in solution, it appears intrinsically disordered [3], and populates a dynamic ensemble of conformations ranging from highly unfolded to fairly compact, for the establishment of stabilizing long-range interactions between the N- and C-terminal regions [4]. Syn exhibits the ability to bind membranes, lipids, and vesicles, and upon binding the protein adopts ordered α-helical structure (Fig. 1B) important to mediate Syn functions correlated to synaptic plasticity, and modulation of neuronal survival [5,6]. Syn structural plasticity is due to the peculiarity of its primary structure, where three regions are distinguishable: the N-terminus (1–60), rich in lysine residues, involved in the binding to negatively charged membranes and lipids [5,7]; the central region (61–95, called NAC, non-amyloid β-component), responsible for the aggregation properties of the protein [8]; and the C-terminus (96–140), containing several acidic residues and prolines, site of post-translational modifications, able to bind metals [9], and to modulate the tendency of the protein to aggregate [10]. N-terminus and NAC, together, (roughly the region spanning residues 1–90), containing imperfect repeats of 11 amino acids with a KTKEGV consensus sequence, resemble the amino acid pattern found in the lipid-binding α-helical domain of the apolipoproteins [11]. The physiological neuronal function of Syn is not fully understood, but there is evidence suggesting its role in

* Corresponding authors.
E-mail addresses: laura.acquasaliente@unipd.it (L. Acquasaliente), patrizia.polverinodelaureto@unipd.it (P. Polverino de Laureto).
[1] Equal contribution

https://doi.org/10.1016/j.ijbiomac.2024.139427
Received 24 October 2024; Received in revised form 18 December 2024; Accepted 30 December 2024
Available online 3 January 2025

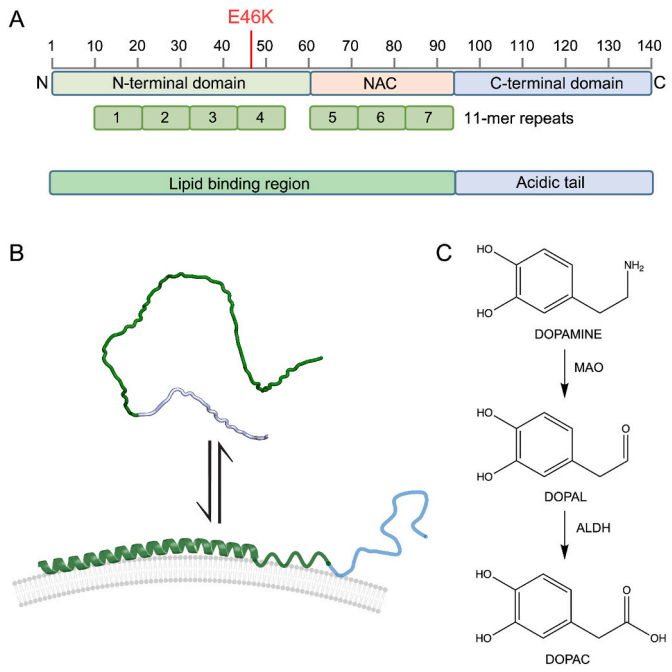

Fig. 1. General model of Syn interacting with a lipid membrane. Primary structure of Syn with indication of the mutation E46K and organization in structural domains (A), scheme showing the conformational transition of Syn in the presence of a lipid membrane (B), structure and generation of DOPAC from Dopamine by enzymatic pathway. MAO indicates Monoamine Oxidase; ALDH indicates Acetaldehyde Dehydrogenase (C).

neurotransmission, modulating the synaptic vesicle dynamics, the mitochondria, and the SNARE complex functions [12]. The protein becomes toxic when it undergoes a transition from a soluble monomer to insoluble fibril, through a progressive process involving oligomer intermediates [13]. Both oligomers and mature fibrils cause toxicity to a different extent and could potentially be linked to the disease [14].

Several missense point mutations of Syn gene have been identified in patients suffering from PD, leading to early-onset (A30P, E46K, A53T, G51D) or late-onset (H50Q) forms of the disease [15]. Although the mutations differently affect Syn aggregation, the precise pathogenic mechanism remains unknown. Multiple lines of evidence indicate that the presence of genetic mutations increases the likelihood of the protein misfolding and, as consequence, its tendency to oligomerization and aggregation [16]. An aspect requiring consideration is that the mutations occur mainly in the region of Syn encompassing the residues from 25 to 97, therefore affecting the protein affinity for and binding modality to lipids. Among the studied mutations, E46K variant has aroused great interest for its high neurotoxicity due to cell-autonomous mechanisms [17] and for the clinical phenotype of E46K patients displaying severe disease progression [14,18]. This mutation also causes changes in the structure of Syn. Indeed, the long-range intramolecular interactions between the N-terminal and NAC with the C-terminal regions result increased and E46K mutant exhibits a more compact than the wild-type protein [19,20]. In relation to the membrane binding property, the K46, located in the middle of the IV of the 7 repeats, induces an increase of the protein affinity to membranes [21], a decreased sensitivity of Syn to membrane curvature [22] and displays a preference for a binding mode to membrane where the residues 3–25 appear tightly linked, while the NAC region is dynamically free and prone to other interactions [23].

Recently, we have studied the molecular interaction between Syn and some plant-derived molecules such as Oleuropein and some structurally related catechols, DOPET and DOPAC [24–26] (Fig. 1C). We showed that these molecules prevent Syn amyloid aggregation in vitro by stabilizing the monomeric form of the protein and inducing the growth of off-pathway oligomers, which do not form fibrils [25]. Catechols exhibit a wide spectrum of biological activities, the ability to cross the blood-brain barrier and are metabolite of dopamine in vivo [27]. Changes in DOPAC levels reflect an alteration of dopamine neurotransmission that may be associated with neurodegenerative disorders like PD [28]. Moreover, DOPAC appears more effective than the hydroxyl-derivative for the presence of the carboxyl negatively charged moiety exhibiting high affinity for the positive charged region of Syn. Cellular assays revealed that the DOPAC-induced oligomers could be internalized into the cell, where they activate the lysosomal pathway and undergo clearance. Finally, these Syn aggregates manifested a reduced propensity to conformational transition in the presence of synthetic membranes in comparison to the monomeric protein. Additional studies were conducted on the mutant E46K by using high-resolution mass spectrometry techniques. Reduced extent of aggregation inhibition by DOPAC was found in the case of E46K [26]. This effect was correlated to the ability of DOPAC to interact preferentially with the protein extended conformers present at the equilibrium with the compact ones in the native state. E46K populates mainly the compact conformer and the interconversion rate between the two species is faster. Finally, these compounds exhibit the property to disaggregate preformed fibrils. Consequently, these molecules could be particularly relevant in the context of neurodegenerative diseases like PD, considering that the symptomatic therapies like levodopa remain the cornerstone treatment and the number of trials for disease-modifying therapies has increased in recent years [29]. In this context, we highlighted how a small molecule scaffold could serve as a model for studying Syn aggregation, its interaction with biological membranes and be proposed for the rationale design of new drugs.

Here, we have studied the effect of DOPAC on the interaction between Syn and E46K with synthetic membranes with the aim to understand the mechanism of binding of the protein in the presence of the catechol. We have used acidic small unilamellar vesicles (SUVs) to generate a model of membrane. Two different settings were studied. In one case, the interaction between the proteins complexed with DOPAC (P/DOPAC) in a previous step and then with SUV (P/DOPAC + SUV) was studied. In a second set of experiments, the catechol was added to the proteins bound to SUV (P/SUV + DOPAC) to evaluate the ability of DOPAC to displace the protein from SUV. In the latter case, two different molar ratios between the proteins and SUV were considered: a "saturating" condition, where the equilibrium bound/unbound protein to SUV is shifted towards the bound protein and a negligible fraction of unbound protein is present and an equilibrium condition, where roughly 50 % of the protein is in the unbound form. These molecular ratios were determined by circular dichroism titration and SPR measurements. Our previous findings demonstrated a two-step reaction between DOPAC and Syn: initially the catechol seems to bind the extended conformation of the protein. Successively, it generates a shield around the molecule. The general effect is a decrease of the long-range intramolecular interactions. Along the aggregation process of Syn, two moments appeared particularly important for the formation of fibril and consequently for their inhibition: the time 0 and 48 h, when the dynamic ratio between the existing different conformers of the molecule determines the speed of aggregation and the ability of certain compounds to inhibit the formation of fibrils [26]. Therefore, in this study the times of incubation 0 and 48 h were chosen to monitor and compare the conformational changes of the proteins in the presence of SUV and DOPAC (condition named +48 h). In summary, our findings reveal that DOPAC plays a significant role in modulating the interactions of both wild-type Syn and the E46K mutant with lipid membranes. By influencing the binding dynamics and conformational states of these proteins, DOPAC not only inhibits fibril formation but also alters the membrane-associated behavior of Syn aggregates. This research enhances our understanding of the molecular mechanisms underlying Syn aggregation and highlights DOPAC as a potential therapeutic agent in the context of PD.

2. Material and methods

2.1. Material and samples

3,4-Dihydroxyphenylacetic acid (DOPAC), Thioflavin T (ThT) and lyophilized bovine catalase (CAT) were purchased from Merck (Darmstadt, Germany). pT7–7 was purchased from Addgene (Watertown, Massachusetts, USA). The catechol powder was dissolved in water solution at 100 mM final concentration and stored at −20 °C [30]. All reagents and chemicals were obtained from Merck (Darmstadt, Germany) and were of analytical reagent grade.

For clarity, the samples used in this study were indicated with a specific name as follows: P, protein (Syn or E46K); P/DOPAC, protein treated with DOPAC (ratio 1:5); P/DOPAC +48 h, protein treated with DOPAC, then incubated for 48 h; P/DOPAC + SUV, protein treated with DOPAC, then incubated with SUV; P/DOPAC + SUV + 48 h, protein with DOPAC, then added to SUV and furtherly incubated for 48 h; P/SUV, protein interacting with SUV; P/SUV + 48 h, protein interacting with SUV and furtherly incubated for 48 h; P/SUV + DOPAC, protein interacting with SUV, then DOPAC is added (displacement); P/SUV + DOPAC +48 h, displacement effect measured over time (48 h).

2.2. Main abbreviations

Syn, α-Synuclein; NAC, non-amyloid β-component; PD, Parkinson's disease; DOPAC, 3,4-dihydroxyphenyacetic acid; DOPET, 3,4-dihydroxyphenylethanol; SUV, small unilamellar vesicle; ThT, Thioflavin T; CAT, bovine catalase; CD, circular dichroism; SPR, surface plasmon resonance; HDX-MS, Hydrogen-Deuterium Exchange Mass Spectrometry; maxD, maximally deuterated sample; MAO, Monoamine Oxidase; ALDH, Acetaldehyde Dehydrogenase;

2.3. Expression and purification of recombinant α-synuclein and its E46K mutant

The expression and the purification of the recombinant proteins α-Synuclein and its E46K mutant were conducted in *E. coli* BL21 and BL21-Gold cells respectively following a procedure previously described [26]. Briefly, the overnight culture of transformed cells was induced with IPTG. All the cultures were performed in LB medium with ampicillin at 37 °C. Osmotic shock was carried out in specific buffers. The periplasmic supernatant was purified using anion exchange chromatography and the eluted fractions were dialyzed and lyophilized. Protein identity and integrity were assessed by ESI-mass spectrometry (MS).

2.4. Small unilamellar vesicle preparation

Small unilamellar vesicles (SUVs) were prepared as reported by Mui et al. [31] L-alpha-Phosphatidylcholine (egg, PC) and L-alpha-Phosphatidylserine (bovine liver, PS) were solubilized in chloroform and mixed at a 1:1 M ratio and dried under gentle stream of nitrogen gas. After 2 h in a SpeedVac vacuum concentrator (Thermo Fisher Scientific, Waltham, MA, USA), the pellet was resuspended in 20 mM sodium phosphate buffer pH 7.4 (previously kept at 37 °C) for 1 h at room temperature. They were vortexed to resuspend the milky and uniform mixture and then subjected to five freeze-thaw cycles. The cycles were performed by vortexing the sample at 37 °C for 2 min, and then freezing it with dry ice. The extrusions were performed with the Liposofast device (Avanti Polar Lipids) by using a 50 nm-polycarbonate membrane. The process was repeated 11 times. The size of SUVs was controlled by dynamic light scattering (Zetasizer Nano-ZS instrument, Malvern, Worcestershire, UK) and the final product was stored at 4 °C.

2.5. Spectroscopic measurements

Protein concentrations were determined by absorption measurements at 280 nm using a double-beam Lambda-20 spectrophotometer (Perkin Elmer Life Sciences). The molar absorptivity at 280 nm for Syn and E46K samples was 5960 cm^{-1} M^{-1}, as evaluated from their amino acid composition by the method of Gill and von Hippel (1989) [32]. The secondary structure content of the proteins was assessed by far-UV circular dichroism (CD). The measurements were performed on a J-800 Series spectropolarimeter (JASCO, Japan) in a 1-mm quartz cuvette at room temperature. Data were recorded in the wavelength range of 250–190 nm, collecting data with high-tension voltage <600 V, and avoiding noisy signals. All protein samples were measured at the same settings averaged in five and the buffer data subtracted. The mean residue ellipticity [θ] (degree cm^2 $dmol^{-1}$) was calculated from the formula [θ] (θ_{obs}/10) (MRW/lc), where θ_{obs} is the observed ellipticity in degrees; MRW is the mean residue molecular weight of the protein; l is the optical path length in cm; and c is the protein concentration in g/mL. A protein concentration of 3–5 μM was used. The spectra were recorded in 25 mM sodium phosphate buffer pH 7.4 in the presence and the absence of liposomes and in the presence and the absence of DOPAC.

2.6. Surface plasmon resonance

Surface Plasmon Resonance (SPR) analyses were performed on a Biacore X-100 dual flow-cell instrument from GE Healthcare using an L1 sensor chip. The chip surface was conditioned with three consecutive 1-minute injections of 20 mM CHAPS followed by 1-minute injection of 30% (V/V) ethanol. SUVs (12 mM in 20 mM Sodium Phosphate buffer, pH 7.4) were deposited for 40 min at a flow rate of 5 μl·min^{-1}. The surface was then stabilized by three 1-min injections of 100 mM NaOH. Aliquots of protein samples at increasing concentrations (0–10 μM) were injected over immobilized liposomes, at 10 μl/min flow rate. All measurements were carried out at 25 °C in 20 mM sodium phosphate buffer, pH 7.4, with 120-sec of contact time and 200-sec of dissociation phase. Liposomes were then regenerated by 1-minute injection of 100 mM NaOH. Each sensorgram was subtracted for the corresponding baseline, obtained on the reference flow cell and accounting for nonspecific binding. Affinity and kinetic analysis were performed using the BIAevaluation software.

2.7. Hydrogen-deuterium exchange mass spectrometry

Hydrogen-Deuterium Exchange Mass Spectrometry (HDX-MS) measurements were performed using a Xevo G2S Q-TOF (Waters) mass spectrometer equipped with a standard electrospray ionization source, an Acquity M-class UPLC (Waters), an Automation 2.0 sample workstation (Waters), and an HDX PAL autosampler (Leap technologies, Carrboro, NC, USA). Leu-enkephalin (Waters) was continuously infused as the reference lock mass. For clarity, the samples used in this study were prepared as follows: P, protein Syn or E46K in PBS buffer; P/DOPAC, protein treated with DOPAC (ratio 1:10) for 1 h at room temperature; P/DOPAC + SUV, protein with DOPAC, then incubated 30 min with SUV; P/SUV, protein incubated with SUV for 30 min at room temperature; P/SUV + DOPAC, protein interacting with SUV, then a 10-fold excess of DOPAC is added (displacement). The final concentrations in the reaction mixture were standardized to 4.8 μM for the protein, 48 μM for DOPAC, and 480 μM for the lipids (SUV), where present. Immediately after the incubation, samples were thermostated at 4 °C. All experiments were conducted in the presence of catalase to prevent oxidation. For the H/D exchange reaction, an aliquot (3 μl) of each sample was diluted 10-fold in deuterated buffer (20 mM sodium phosphate, pD 7.42, in 99.9 % D_2O) and was then allowed to exchange for 5 s or 10 min at 4 °C. H/D exchange was quenched at 0 °C by adding an equal volume of quenching buffer, i.e. 0.8 % formic acid, adjusted to pH 2.35. Quenched samples were immediately digested on an in-line pepsin column (Enzymate™ BEH Pepsin Column, Waters), thermostated at 15 °C and eluted at a constant flow rate (100 μl/min) with 0.23 % (v/v) aqueous formic acid. The resulting peptic fragments were online trapped

on an Acquity UPLC BEH C18 VanGuard Pre-column (Waters) and eluted on an Acquity UPLC BEH C18 column (Waters) with a linear acetonitrile-0.1 % formic acid gradient from 5 % to 35 % in 6 min, at a constant flow rate of 40 μl/min. The effluent was analyzed by the Xevo G2S Q-TOF mass spectrometer (*m/z* 50–2000), and each peptic fragment was identified by the MS^E mode, using argon as the collision gas. Deuterium incorporation was determined according to the following equation [33]: $\%D = (m_t - m_0)/(m_{100} - m_0)$, where m_t is the mass of the fragments after labeling time t, m_0, and m_{100} are the masses of the non-deuterated fragment and the maximally deuterated sample (maxD), respectively. The maximally deuterated samples used for back-exchange corrections were prepared as described by Peterle et al. (2022) [34]. Briefly, proteins were lyophilized, suspended in 7 M GdnHCl, and heated at 90 °C for 5 min. After cooling to room temperature, the labelling buffer was added to the denatured protein solution, obtaining a final 95 % of D_2O, and the exchange reaction proceeded at 40 °C for 10 min. The samples were then cooled to room temperature, and the exchange was quenched by two-fold dilution with an ice-cold quenching buffer (as above). Fragments generated from online pepsin digestion were identified using the Protein Lynx Global Server 3.0 and then analyzed with DynamX 3.0 software (Waters). Only fragments matching the following criteria were considered for the analysis: i) 5 %-retention time window in the chromatographic separation; ii) maximum MH^+ error of 6 ppm; iii) at least 2 ion products identified for each peptic fragment; iv) a minimum of 0.2 ion products generated per amino acid in the fragment; v) fragments containing <4 or >33 amino acids were excluded, due to identification ambiguity and poor sequence localization.

2.8. Cell culture conditions and treatments

Human neuroblastoma SH-SY5Y cells were cultured at 37 °C in a humidified incubator under a 5.0 % CO_2 atmosphere in 50:50 HAM: DMEM culture medium supplemented with 10 % fetal bovine serum, 3.0 mM glutamine, 100 units/mL penicillin and 100 μg/mL streptomycin. Cells were exposed for varying lengths of time to protein samples (5 μM Syn or E46K) aggregated in vitro for 48 h in the absence or presence of DOPAC.

2.9. Mitochondria functionality

The MTT reagent (3-(4,5-dimethylthiazol-2-yl)-2,5-diphenyltetrazolium bromide (Sigma-Aldrich, St. Louis, MO, USA) was added to SH-SY5Y cells seeded in 96-well plates (1×10^4 cells/well) at a final concentration of 0.5 mg/mL. After incubation for 2 h at 37 °C, formazan crystals formed from MTT by the reducing activity of mitochondrial dehydrogenases were dissolved with 100 μl solubilizing solution (DMSO) and the absorbance of the blue formazan resulting from MTT reduction was read at 595 nm using a Biotek Synergy 1H spectrophotometric plate reader.

2.10. Reactive oxygen species measurements

The probe 2′,7′-dichlorofluorescein diacetate, acetyl ester (CM-H DCFDA; Sigma-Aldrich) was added at a final concentration of 10 mM to SH-SY5Y cells plated in 96-well plates (1×10^4 cells/well). After 1 h, fluorescence values were read at 538 nm using a Biotek Synergy 1H spectrophotometric plate reader.

2.11. Interaction with cell membrane

Subconfluent SH-SY5Y cells (8×10^4 cells/well) grown on glass coverslips were treated for 24 h with Syn aggregates at a 5.0 μM final concentration and then washed with PBS. Cell nuclei were stained with HOECHST 33342 for 30 min at 37 °C. Ganglioside M1 (GM1) labeling was performed by incubating the cells with 10 ng/mL CTX-B Alexa Fluor 488- conjugated in complete medium for 10 min at room temperature. Cells, fixed in 2.0 % buffered paraformaldehyde for 10 min, were permeabilized by treatment with a 1:1 acetone/ethanol cold solution for 4.0 min at R.T., washed with PBS and blocked with blocking solution (PBS, 0.5 % BSA and 0.2 % gelatine) for 30 min. After blockage, the cells were incubated for 1 h at room temperature with a rabbit polyclonal anti-Syn antibody (Abcam, Cambridge UK) diluted 1:500 in blocking solution and then washed with PBS for 30 min under stirring. The immunoreaction was revealed by Alexa 568-conjugated anti-rabbit Abs (Molecular Probes, Eugene, Oregon, USA) diluted 1:100 in PBS. Cell fluorescence was imaged using a confocal TCS SP8 scanning microscope (Leica) equipped with 63×, 1.4–0.6 NA, oil, HCX Plan APO lens. Multicolor images were analyzed with FiJi software. Förster Resonance Energy Transfer (FRET) analysis was carried out by the FRET sensitized emission method as previously reported [35].

2.12. Calcium flux

Cytosolic levels of free Ca^{2+} were measured using the fluorescent probe Fluo-3 acetoxymethyl ester (Fluo-3 AM; Molecular Probes). Subconfluent neuroblastoma cells (8×10^4 cells/well) grown in complete or free Ca^{2+} medium, on glass coverslips were loaded with 5.0 μM Fluo-3 AM at 37 °C for 15 min and then treated with different protein samples for 2 h. Finally, the cells were fixed in 2.0 % paraformaldehyde in PBS for 10 min. Imaging was performed using a Leica TCS SP8 confocal scanning microscope with a Leica Plan 7 Apo 40× oil immersion objective. The Ca^{2+} flux was monitored in SH-SY5Y cells, plated on 96-well plates at a density of 1×10^4 cells/well and labelled as previously described, before exposing to different aggregates. The fluorescence intensity of Fluo3-AM was monitored continuously at 526 nm for 2 h from the moment the protein samples were added to the cell medium using a Biotek Synergy 1H plate reader.

2.13. Statistical analysis

All data were reported as mean values ± standard deviation (SD) of biological triplicates for HDX-MS analysis. Statistical analysis using one-way ANOVA, with *p*-value <0.05 as regarded statistically significant. The differences between control and experimental samples were determined by *t*-test. One-way analysis of variance by ANOVA and pairwise comparisons by the Tukey HSD (honestly significant difference) method were used for the statistical evaluation of the cellular assays.

3. Results

3.1. Interaction of Syn and its mutant with SUV (P/SUV) probed by circular dichroism and surface plasmon resonance

It is widely accepted that Syn exists in vivo as an equilibrium between the free unfolded and membrane-bound α-helical forms [36,37]. A stable system was developed to mimic neuronal biological membranes, which are natural targets for Syn. Small unilamellar vesicles (SUVs) consisting of negatively charged phospholipids, with a diameter of 50–80 nm, were chosen as Syn preferentially binds to lipids that contain negatively charged polar head groups, with a strong preference for phosphatidylserine (PS), because of the electrostatic attraction between the anionic membrane surface and the cationic lysine-rich N-terminus domain [38]. The chosen system exhibited stability for all the time range used to perform the experiments (Fig. S1). In vitro, the molecular ratio between the two forms (bound and unbound) can be modulated by changing the lipid composition and concentration of SUVs[38]. Increasing the SUV concentration with respect to the protein, the bound/unbound protein equilibrium is shifted towards the bound form. Here, in the first set of experiments, a protein/SUV (P/SUV) molar ratio was determined to minimize the percentage of free molecules in equilibrium with the bound ones (saturating condition). The endpoint of the titration was calculated as the molar concentration of the SUV, with

whom no further changes of the protein secondary structure were detectable. The conformational changes of the proteins from unfolded to α-helical structure was monitored by far UV CD measurements (Fig. 2 A and B). The CD spectra of Syn and E46K showed a clear transition from the unstructured free form to the α-helical bound species, where two typical minima at 208 and 220 nm were visible. The CD spectra of both proteins formed an isodichroic point at 204 nm, suggesting a cooperative folding process on the SUV surface. The saturation point was calculated as the first P/SUV molar ratio displaying the maximum molar ellipticity at 222 nm and it was 1:500 for Syn and 1:300 for E46K. Plotting the normalized ellipticity as a function of SUV concentration (Fig. 2C), E46K lipid-induced folding appears more rapid than that of the wild-type molecule, in agreement with previous results [22].

The binding affinities for the interaction of Syn and its mutant with SUV were determined by SPR analysis (Fig. 2D-F). In these measurements, SUVs with identical composition to CD experiments were captured on the L1 sensor chip and left to interact with Syn and E46K. The two proteins exhibited a comparable affinity (K_{dSyn} 38 ± 5 μM and K_{dE46K} 32 ± 2 μM), but different kinetics of association/dissociation to/from membrane. Notably, the two K_d calculated at the equilibrium (Fig. 2F) are comparable to those calculated from kinetic analysis as the ratio of k_{off}/k_{on}. SPR curves were interpolated according to a single-binding kinetic model with best-fit parameters: Syn, k_{on}: 5863 M^{-1} s^{-1}, k_{off}: 0.158 s^{-1}, K_d: 26.9 μM; E46K, k_{on}: 1605 M^{-1} s^{-1}, k_{off}: 0.0406 s^{-1}, K_d: 25.3 μM. For Syn, faster association (k_{on}) and dissociation (k_{off}) rate constants were calculated compared to those determined in the interaction E46K/SUV. The extra positive charge in the lipid binding domain due to substitution E → K at position 46 is expected to favor the protein interaction with negatively charged lipids, but it was also suggested that the electrostatic factor promoted by E46K mainly affects the dissociation rate from the SUV surface [21].

3.2. Interaction of P/DOPAC with SUV probed by circular dichroism and Hydrogen Deuterium Exchange (HDX) - mass spectrometry (MS) measurements. (P/DOPAC + SUV)

Two series of experiments have been carried out. In one set, the interaction between the proteins incubated with DOPAC (P/DOPAC) and SUV in comparison to the protein/SUV (P/SUV) interaction was studied. The protein/DOPAC ratio (1:5) was selected on the basis of our previous research and corresponds to an amount of catechol able to provide the complete inhibition of the aggregation of the protein [25]. In another one, the effect of adding DOPAC to the protein bound to the SUV was analyzed. In the first case, the samples are named P/DOPAC + SUV, while in the second P/SUV + DOPAC. In addition, the samples P/DOPAC were incubated for 48 h before mixing with SUV (P/DOPAC +48 h + SUV) as a further assay. After 48 h-incubation in the presence of catechol, Syn and E46K generated oligomeric forms [26], therefore the interaction between 48 h-species grown in the absence or in the presence of DOPAC was tested. The protein conformational and dynamics changes were monitored by using far-UV CD and HDX-MS measurements.

Far UV CD spectra were recorded immediately after the preparation of the samples constituted by the protein and DOPAC (P/DOPAC) in the presence and in the absence of the SUV. As was previously reported [25], DOPAC does not induce evident conformational changes (Fig. 3A, C, continuous black lines), and both proteins adopt the unfolded structure as in the absence of the catechol (Fig. 3A, C, dashed black lines). The species formed by the protein and DOPAC (1:5 P/DOPAC) were then mixed to SUV (1:500 for Syn/SUV; 1:300 for E46K/SUV). Far-UV CD spectra gave indication of acquisition of α-helical structure by protein/DOPAC species suggesting their ability to bind to the lipid membrane, similarly to the protein alone (Fig. 3A, C, red continuous lines). Both proteins, Syn and E46K mixed with DOPAC underwent conformational transition in the presence of SUV at similar extent (Fig. 3, continuous red

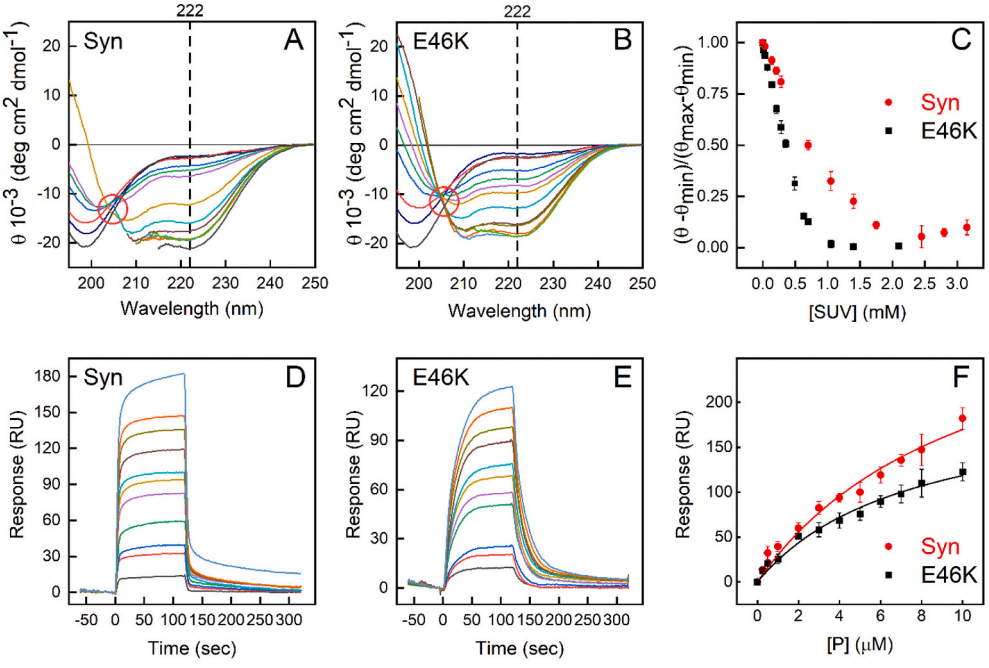

Fig. 2. Interaction of Syn and E46K with the SUV membrane probed by CD and SPR. Far-UV CD spectra of Syn (A) and E46K mutant (B) at increasing SUV concentrations. Representative spectra were reported. Protein concentration was 3.5 μM. The isodichroic point was highlighted. The normalized ellipticity at 222 nm obtained from three independent measurements was plotted against the SUV concentration (C). SPR curves obtained at increasing concentrations of Syn (D) and E46K (E). The measurements were carried out at 25 °C in a 20 mM sodium phosphate buffer pH 7.4. SPR curves were interpolated according to a single-binding kinetic model with best-fit parameters: Syn, k_{on}: 5863 M^{-1} s^{-1}, k_{off}: 0.158 s^{-1}, K_d: 26.9 μM; E46K, k_{on}: 1605 M^{-1} s^{-1}, k_{off}: 0.0406 s^{-1}, K_d: 25.3 μM. (F) Steady state affinity determination. Plot of the response at equilibrium as a function of protein concentration and fitting for 1:1 binding model. The affinity constants are K_d: 38 ± 5 μM for Syn and K_d: 32 ± 2 μM for E46K.

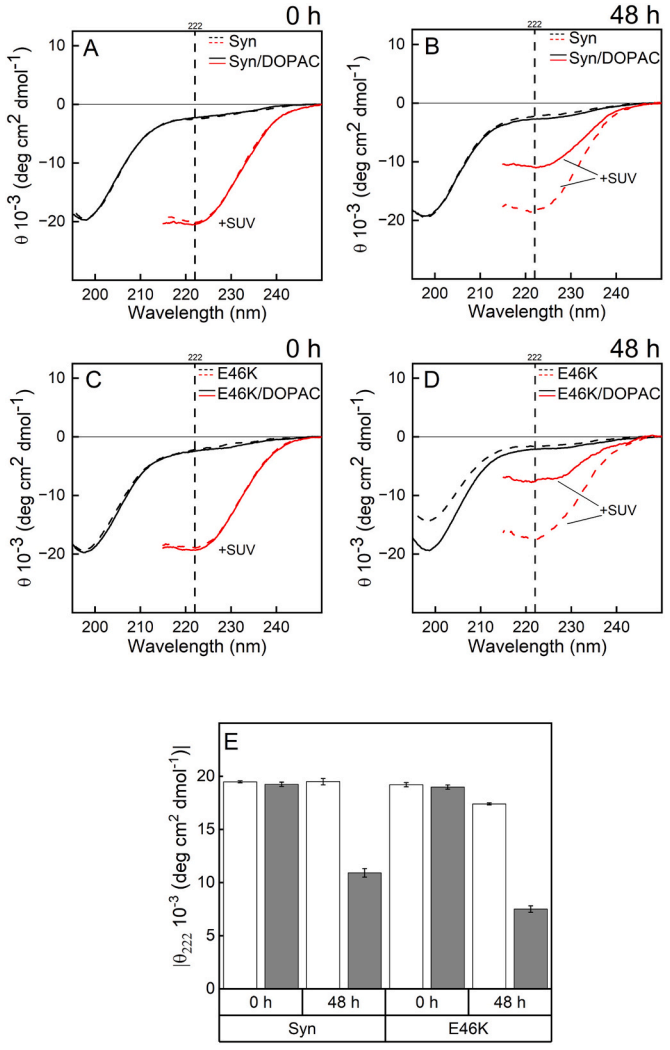

Fig. 3. Interaction of Syn and E46K mixed with DOPAC (P/DOPAC) with SUV at time 0 (A, C) and of P/DOPAC species formed after 48 h of incubation (P/DOPAC +48 h) with SUV (B, D) probed by far-UV CD. SUV concentration was selected to obtain negligible fraction of unbound protein. The plots show the proteins in the presence (solid black line) and in the absence (dashed black line) of DOPAC, and the proteins in the presence (solid red line) and in the absence (dashed red line) of DOPAC incubated with SUV, respectively for Syn (A, B) and E46K (C, D). In E, the bars report the ellipticity (in absolute value) at 222 nm of the spectra in red. The black bars refer to the ellipticity of the samples P/DOPAC mixed with SUV in comparison to P/SUV (white bars).

lines). Successively, P/DOPAC samples were incubated for 48 h and then mixed with SUV (Fig. 3B, D). A decreased ellipticity was detected in the case of E46K/DOPAC, correlating to the presence of a higher amount of oligomeric species than in the case of Syn as previously shown [26]. In the presence of DOPAC and SUVs, the ellipticity is lower (red continuous lines) than in the presence of SUVs alone (red dashed lines). This effect is more remarkable for E46K/DOPAC than the wild-type protein. These data suggested that the complex formed by the proteins and the catechol incubated for 48 h (P/DOPAC +48 h) exhibits a reduced affinity for SUV (Fig. 3B, D).

H/D exchange measurements by MS of Syn and its mutant E46K complexed with DOPAC were then performed in the presence and absence of lipid membranes in comparison to P/SUV systems. Firstly, the experiments were conducted by measuring the percentage of H/D exchange for 5 s of Syn and E46K in the presence of the SUV (Fig. 2S). The profiles were compared with those obtained from the proteins alone that, as completely unfolded species appeared fully deuterated.

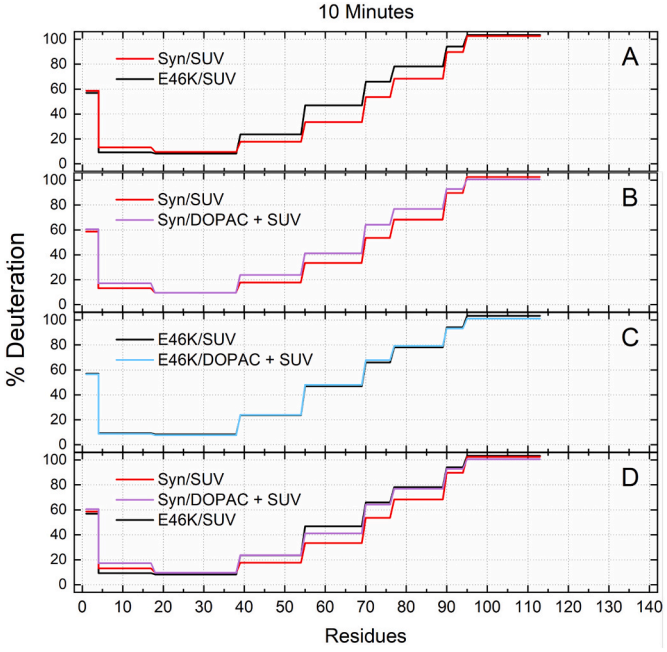

Fig. 4. Interaction of Syn and E46K in presence of DOPAC (P/DOPAC) with SUV probed by HDX-MS. Percentage of deuteration of Syn (red line) and E46K (black line) in the presence of SUV (P/SUV) (A). Comparisons of the percentage of deuteration of Syn/SUV (red line) and Syn/DOPAC + SUV (purple line) (B), and E46K/SUV (black line) and E46K/DOPAC + SUV (light blue line) (C). To highlight the effect of DOPAC, to the profiles shown in B relative to E46K/SUV was added (D). All these profiles were obtained by 10 min of exchange.

Allowing the deuteration for 5 s (Fig. 2S), there was no appreciable difference in the profiles obtained for both proteins that showed a similar behavior. In the presence of SUV, the 1–94 region of the polypeptide chain exchanged very poorly (4–5 %), a second stretch of the protein sequence (95–113) exchanged in a higher extent (60–64 %), while the segment corresponding to the C-terminus (114–140) appears quite flexible and exchanged very extensively, in agreement with other models of Syn interacting with membranes [6,39]. Deuterium incorporation was then prolonged to 10 min (Fig. 4). When Syn and E46K were analyzed in the presence of SUV, the region 18–38 showed a lower deuterium incorporation by 10 % in both proteins, while substantial differences between the two proteins were observed in the region 40–95. Within this region, the segment 55–70 exhibited a significant variation by 30 % in the wild type and by 50 % in the mutant when exchanging H with D (Fig. 4A). The presence of DOPAC added to Syn before the interaction with the membrane (P/DOPAC + SUV) increased the exchange in the 40–90 region, thus its mobility, making the behavior of Syn more like that of the mutant (Fig. 4B). Fig. 4C instead shows the comparison between E46K and E46K/DOPAC with the SUV. In this case, unlike Syn, there was no exchange difference. To better compare the effect of DOPAC on the interaction of the protein with membranes, in Fig. 4D, the percentage of deuteration of the complex Syn/DOPAC with SUV was reported in relation to the exchange of the wild-type and mutant with SUV in the absence of the catechol. The 55–70 region of Syn bound to DOPAC appeared more prone to exchange than when the protein is directly bound to the membrane, but less than in the case of E46K.

3.3. Effect of DOPAC on the interaction of Syn and its mutant with SUV (P/SUV + DOPAC) probed by circular dichroism and Hydrogen Deuterium Exchange (HDX) - mass spectrometry (MS) measurements

Having tested the affinity of P/DOPAC to SUV, a new experiment was performed by adding DOPAC after the establishment of the interaction

between the proteins and the lipid membrane (named P/SUV + DOPAC), to assess if the catechol was able to displace the protein from the membrane. In this case, two different protein/SUV ratios were considered: one in which the percentage of free protein molecules is negligible and another one in which 50 % of the protein is in the bound form. These ratios were chosen based on the results shown in Fig. 2.

In Fig. 5, the effect of DOPAC on the interaction of the proteins with SUV (saturation P/SUV ratio) at time 0 (P/SUV + DOPAC) and after 48 h-incubation (P/SUV + DOPAC +48 h) was shown. The CD spectra of the proteins in the absence and in the presence of DOPAC without SUV were reported as a control (Fig. 5, dashed and continuous black lines). At time 0, both Syn and E46K acquired α-helical structure in the presence of the SUV, as already shown in Fig. 2. The ellipticity of the CD curves at 222 nm for both wild type and mutated proteins was similar (Fig. 5A, C, dashed red lines; E, white bars). This did not change after 48 h-incubation in quiescence (Fig. 5B, D, dashed red lines; E, white bars), suggesting that the system formed by the protein and SUV was stable under these experimental conditions. Upon adding DOPAC (in ratio 1:5 calculated on the protein concentration), a slightly reduced content of the α-helical structure of the proteins was detected at time 0 (Fig. 5A, C, continuous red lines). After 48 h of incubation, the α-helical content was even more reduced for E46K (Fig. 5B, D, continuous red lines; E, black bars), while no significant change was detected for the wild type protein.

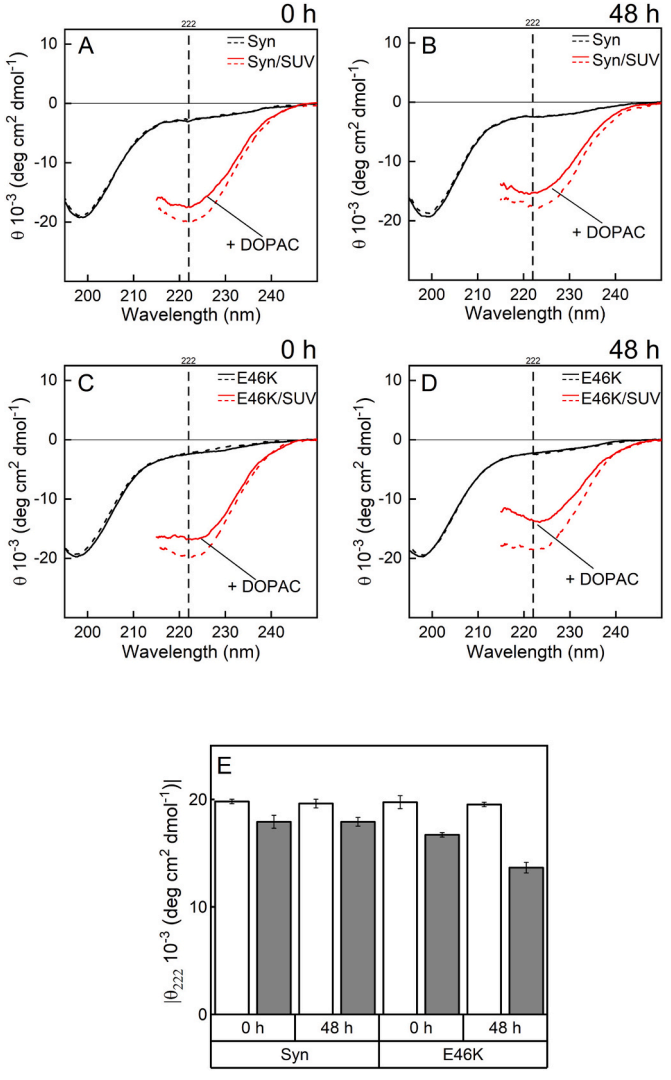

Fig. 5. Effect of DOPAC on the interaction of Syn (A, B) and E46K (C, D) with SUV (P/SUV) at time 0 (A, C) and 48 h (B, D) probed by far-UV CD. SUV concentration was selected to obtain negligible fraction of unbound protein. The curves relative to the protein with SUV in the absence of DOPAC were reported as dashed red lines. DOPAC was added to obtain a final molar ratio of 1:5 (P/DOPAC 1:5, continuous red lines). The 48 h-incubation was performed without shaking the samples. The CD curves of the protein in the absence of SUV were reported as a control (in the absence of DOPAC, dashed black lines; in the presence of DOPAC, continuous black lines). In E, the bars report the ellipticity (in absolute value) at 222 nm of the spectra in red. The black bars refer to the ellipticity of the P/SUV samples upon addition of DOPAC, the white bars report the ellipticity of the P/ SUV samples as a control.

HDX-MS measurements were conducted to understand if the reduced content of ellipticity could be ascribable to a protein displacement from the lipid membrane or a partial unfolding of a specific region of the protein after the addition of DOPAC to the proteins bound to SUV. These measurements were conducted only on freshly prepared samples, without further incubation to avoid that eventual protein aggregative processes could interfere in the MS measurements. In the case of Syn, no difference in the HDX-MS profiles was detectable (Fig. 6A). Conversely, the H/D exchange of the mutant bound to SUV was largely affected by the catechol at the level of the 40–89 region (Fig. 6B). The biggest difference was found for the 55–70 segment where the H/D exchange changed from 50 to 70 % (Fig. 6C).

To clarify the catechol preference for the bound or unbound form of the protein, DOPAC was added to P/SUV at an SUV concentration allowing the presence of a large fraction of unbound protein (50 %). Therefore, for Syn, a 1: 140 P/SUV ratio was chosen, while for E46K, this ratio was 1:100. In these conditions, DOPAC could interact with the fraction of free protein or displace the protein from the membrane. The analysis was monitored by CD at time 0 and 48 h. First, the stability of the system constituted by the protein bound to the SUV was tested over 48 h, detecting no change in the ellipticity (Fig. 7B, D, dashed red lines; E, white bars). The addition of DOPAC at time 0 induced a slight effect both in the case of Syn and E46K, being the most pronounced in the case of the mutant after 48 h-incubation (Fig. 7, continuous red lines; E, black bars). Overall, these measurements show that DOPAC seems to be more effective in reducing the interaction of E46K with the membrane.

Finally, the effect of further addition of DOPAC was tested. The system used was constituted by the protein bound to SUV incubated for 48 h without agitation in the absence (P/SUV + 48 h, Fig. 8 A, C, dashed blue lines; B1, D1, blue bars) or in the presence (P/SUV + DOPAC +48 h,

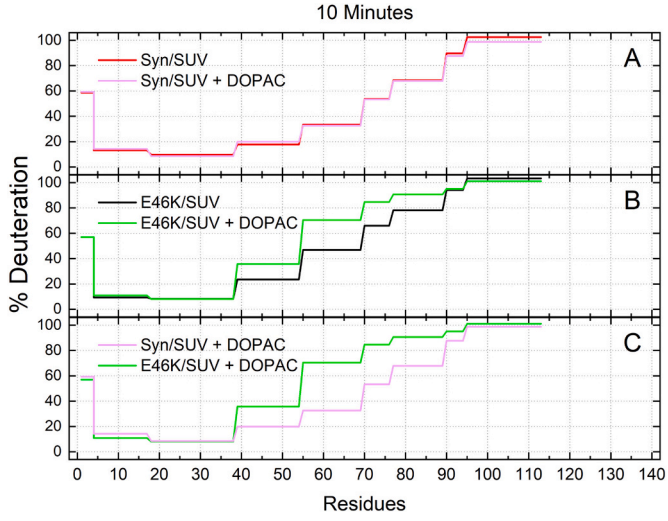

Fig. 6. Effect of DOPAC on the interaction of the proteins with SUV probed by HDX-MS. Percentage of deuteration of Syn/SUV upon addition of DOPAC (pink line) in comparison with the profile of Syn/SUV (red line) (A). Percentage of deuteration of E46K/SUV upon addition of DOPAC (green line) in comparison with the profile of E46K/SUV (black line) (B). Comparison of percentage of deuteration of P/SUV upon addition of DOPAC (pink and green line, respectively for Syn and E46K) (C). The profiles were obtained by 10 min of exchange.

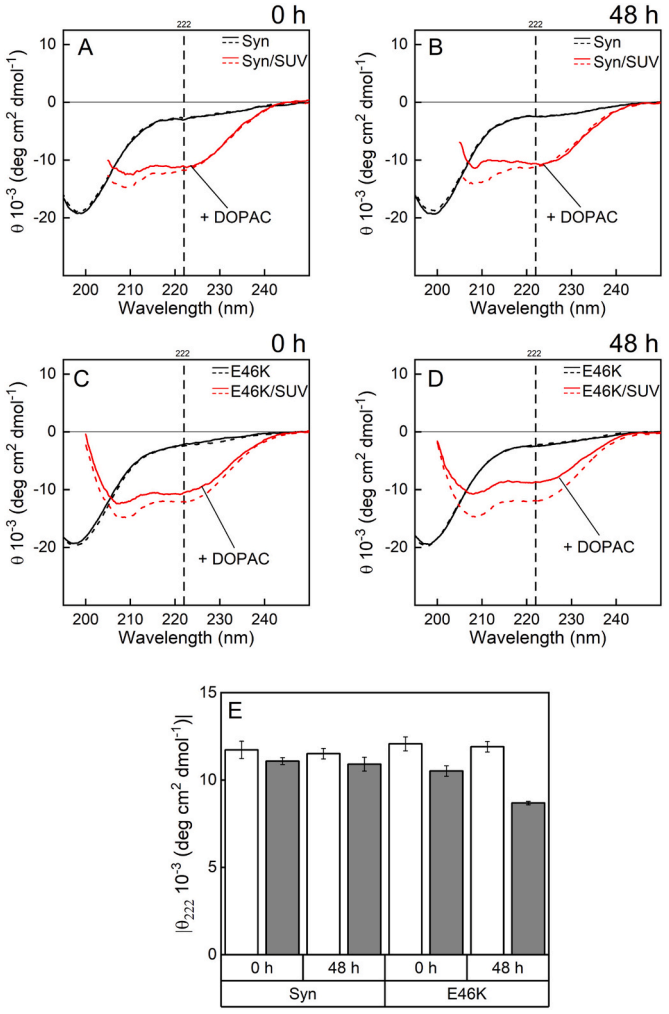

Fig. 7. Effect of DOPAC on the interaction of Syn (A, B) and E46K (C, D) with SUV (P/SUV) at time 0 (A, C) and 48 h (B, D) probed by far-UV CD. The molar ratio Syn/SUV was 1:140; the molar ratio E46K/SUV was 1:100, to have 50 % of the protein in the bound form. The curves of the protein with SUV in the absence of DOPAC were reported as dashed red lines. DOPAC was added to obtain a final ratio of 1:5 (P/DOPAC 1:5, continuous red lines). The 48 h-incubation was performed without shaking the samples. The CD curves of the protein in the absence of SUV were reported as a control (in the absence of DOPAC, dashed black lines; in the presence of DOPAC, continuous black lines). In E, the bars report the ellipticity (in absolute value) at 222 nm of the spectra in red. The black bars refer to the ellipticity of the P/SUV samples upon addition of DOPAC, the white bars report the ellipticity of the P/ SUV samples as a control.

Fig. 8 A, C, continuous blue lines; B2, D2, blue bars) of DOPAC. DOPAC could react with the fraction of free protein in equilibrium with the bound one and with protein displaced from the SUV. A decrease of ellipticity was detected, more pronounced in the case of E46K. As a control, a fresh protein sample (3.5 μM) was added to both systems to verify the occurrence of a competition event between the free protein, SUV and available DOPAC (Fig. 8, green lines, and green bars). The addition of new protein molecules restored only in part the initial content of α-helical structure, even less in the case of E46K.

3.4. Protein aggregate effects on cultured cells

The interaction between Syn and cell membrane can lead to its permeabilization with loss of membrane integrity, but also to dysregulation of calcium signaling and consequent production of reactive oxygen species (ROS) [40,41], which are both involved in neuronal toxicity. Indeed, Syn aggregates, particularly in their oligomeric form, could permeabilize the neuronal membranes by destabilizing the lipid bilayer and forming transient pores [42]. Therefore, a series of analyses on a human neuroblastoma cell line were performed. SH-SY5Y cells, which are a well-characterized cell model for neurodegeneration studies, were used to investigate Syn aggregates interaction with cells. The toxicity of exogenous Syn and E46K aggregates obtained after 48 h of aggregation in vitro in the absence and presence of catechol (P + 48 h and P/DOPAC +48 h) were tested.

First, we evaluated the aggregates/cell membrane interaction by confocal microscopy analysis. The interaction between exogenous Syn or E46K aggregates, with or without DOPAC, and GM1, a ganglioside present in neuronal membrane was observed in terms of colocalisation (Fig. 9A, top panels) and sensitized Förster resonance energy transfer (FRET) confocal analyses (Fig. 9A, bottom panels). The Syn and E46K aggregates on cells showed a remarkable colocalisation with GM1 in the plasma membrane (Fig. 9A, top panels) and an intense FRET interaction between GM1 staining (Alexa488-conjugated cholera toxin, subunit B) and Syn immunolabeling (Alexa568) was observed (Fig. 9A, top panels). On the other hand, the few DOPAC-modified aggregates detected on the cell showed a low FRET efficiency between Alexa488 and Alexa568 (Fig. 9A, lower panels).

To investigate how the different aggregates may affect cell membranes integrity, the change in intracellular calcium levels was assessed. Cells were treated for two hours with the different types of protein aggregates grown in the presence or absence of DOPAC, after which the confocal microscopy images of the cells loaded with the Fluo3-AM probe were recorded. Fig. 9B shows increased Fluo3-AM fluorescence in cells treated with the Syn and E46K aggregates, while the DOPAC-modified aggregates caused no change in intracellular calcium levels. This result was confirmed by a further in vivo cell analysis of intracellular calcium levels by treating the cells with the aggregates and immediately initiating fluorescence recording for the next two hours. An increase in intracellular calcium levels was observed approximately 45 min after treatment of the cells with Syn and E46K (Fig. 9C). This change was not recorded when the experiments were performed in Ca^{2+}-depleted medium, demonstrating that these aggregates increase the uptake of external Ca^{2+} and thus destabilize membrane permeability. When cells were treated with DOPAC-modified aggregate protein samples with low affinity for the cell membrane, no change in calcium levels was recorded (Fig. 9C).

Mitochondrial impairment linked to membrane destabilization was assessed by the ability of cells to reduce the MTT probe (Fig. 9D) and the production of reactive oxygen species (ROS) using a fluorescent ROS indicator (DCFDA) (Fig. 9E). Syn and E46K aggregates resulted in a significant reduction in mitochondrial function, compared to untreated control cells, and increased levels of ROS were observed, indicating oxidative stress induced by the aggregates. Consistent with literature reports, E46K aggregates exhibited greater toxicity than Syn aggregates [43]. Notably, there was no significant difference in toxicity between 4-h and 24-h treatment for both proteins. This suggests that the cytotoxic effects may occur rapidly upon interaction with cell membranes. When cells were treated with P/DOPAC +48 h, a reduced cell sufferance and a corresponding decrease in ROS production were observed, suggesting that the protein/DOPAC complexes exhibit lower toxic activity (Fig. 9D, E). Taken together, these results not only support the in vitro data, but also highlight the potential of DOPAC as a protective agent, suggesting that DOPAC-induced modifications may alter the mechano-physical properties of the aggregates potentially mitigating their toxic effects on neuronal membranes.

4. Discussion and conclusion

Syn is engaged with lipids as a part of its physiological and pathological function [44]. Several factors affect Syn-lipid interaction such as

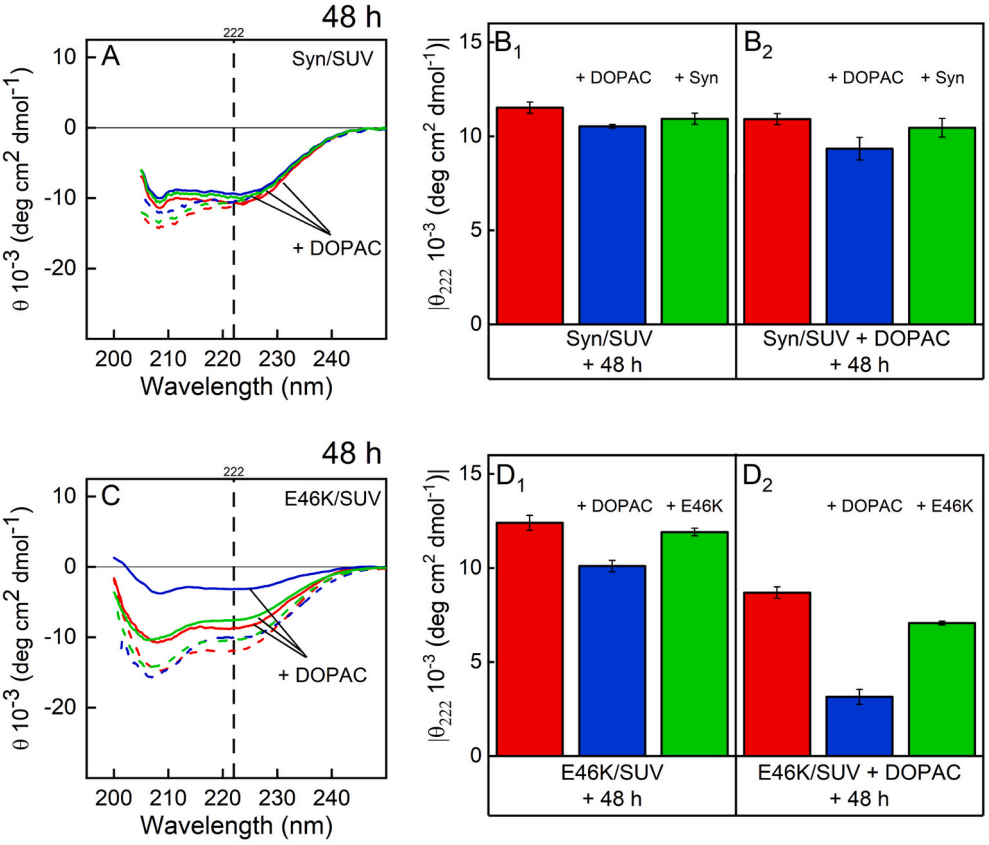

Fig. 8. Effect of further addition of DOPAC on the interaction of Syn (A, B) and E46K (C, D) with SUV (P/SUV) after 48 h without shaking. SUV concentration was selected to have 50 % of the protein in the bound form. To the samples P/SUV + DOPAC +48 h (continuous red lines, A, C; red bars, B_2, D_2), DOPAC in ratio 1:5 with the protein was added (P/SUV + DOPAC +48 h + DOPAC, continuous blue lines, A, C: blue bars, B_2, D_2). In comparison, DOPAC was added to P/SUV + 48 h (dashed red lines, A, C; red bars, B_1, D_1) in the same ratio (P/SUV + 48 h + DOPAC, dashed blue lines, A, C; blue bars, B_1, D_1). Continuous green lines (A, C) and green bars (B_2, D_2) refer to samples as described for the blue lines and bars to which fresh protein (3.5 μM) was added (P/SUV + DOPAC +48 h + DOPAC + P). The dashed green lines (A, C) and green bars (B_1, D_1) refer to P/SUV + 48 h + DOPAC + P.

the composition of the lipid system and the reciprocal concentration of the protein and the lipid [45]. It is quite difficult to assess all the aspects contributing to this interaction, since lipid vesicles can also trigger Syn aggregation and fibril formation [38] and lipids themselves are in vivo constituents of the Lewy bodies, pathological hallmarks of PD [46]. Therefore, we decided to focus our study on the dynamics of the Syn/membrane interaction by using biophysical approaches. Previously, we have shown that Syn and E46K aggregation is inhibited by DOPAC in a dose-dependent manner and that the mutant requires higher concentrations of the compound than Syn for the complete inhibition. DOPAC seems to recognize the extended conformation of the protein among the interconverting ones present at equilibrium preventing long-range interactions responsible for the packed conformation. The aggregation-prone species is thus confined in a non-aggregating one and the intramolecular aggregation process is hampered [26]. Here, we analyzed how protein/DOPAC complexes interact with SUV and the effects of DOPAC on already membrane bound protein. Overall, our findings provided a dynamic model of interaction of Syn and E46K with the membrane able to explain the different behavior of the two proteins in relation to the amyloid inhibitor.

Far-UV CD and SPR measurements were employed to assess the ability of the two proteins to bind membranes and to determine the saturation conditions (negligible fractions of unbound proteins). Measurements obtained by far UV-CD showed the ability of the proteins to assume a different content of α-helical secondary structure in relation to the protein-liposome ratio. The existence of an isodichroic point at ~205 nm indicates the presence of two different populations in equilibrium and a cooperative folding process [47]. Indeed, the presence of a single molecule structured on the membrane may reduce the free energy required for the second molecule to structure itself. E46K lipid-induced folding appears more rapid than Syn and the mutant requires less lipid concentration to complete its conformational transition. A P/SUV ratio of 1:500 for Syn and 1:300 for E46K were found to be the saturating conditions. The lower saturation ratio for E46K than Syn suggests a higher avidity of the mutant for this type of membrane or a different modality of binding. The positively charged Lys46, as well as intensifying the binding to the negatively charged surface of the liposome, shifts the bound-unbound equilibrium towards the bound form of the protein, as previously proposed [22]. Interestingly, Syn and E46K exhibit similar affinity to membrane but different kinetics of interaction. The association (k_{on}) and dissociation (k_{off}) constants calculated for Syn have a higher value than those calculated for E46K. Since k_{on} and k_{off} are indices of the time required to reach equilibrium in the interaction between the protein and the lipid vesicle, they confirm that the mutant needs more time to acquire the secondary structure. The binding of Syn to SUV occurs in a concentration dependent manner and with an affinity (K_d) in the micromolar range, as determined by SPR, comparable to those reported elsewhere using anionic lipids. In addition, K_d of this magnitude suggests that the protein is in a monomeric state; a partially aggregated or oligomeric species of Syn should be characterized by a submicromolar affinity constant [48]. Of note, at higher concentrations (i.e., 10 μM) Syn appears stably bound on the SUV surface, even after 3 min of the dissociation period. This suggests that Syn not only interacts with the anionic lipid head groups but also could insert deeper into the lipid bilayer, as previously suggested [49].

The binding model of Syn and E46K to SUVs determined by HDX-MS

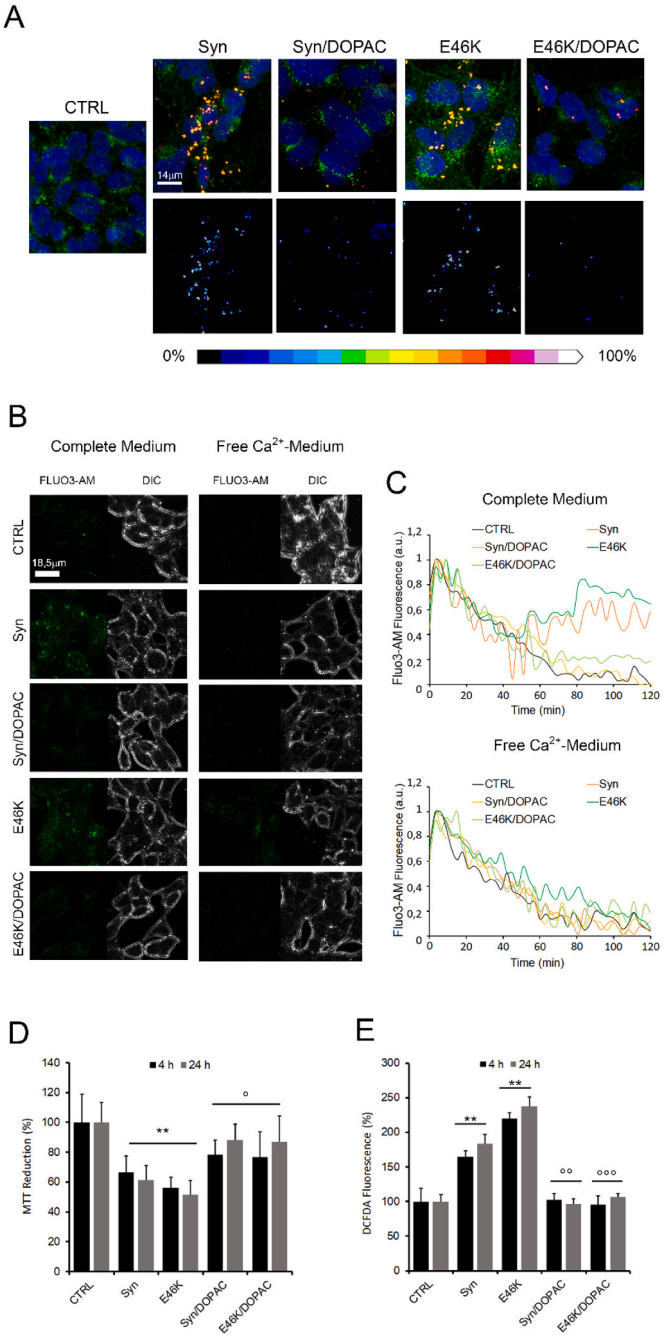

Fig. 9. Interaction of Syn and E46K aggregates with cells. SH-SY5Y cells were treated for 24 h with Syn or E46K aggregates, obtained after 48 h of incubation in the absence or in the presence of DOPAC (P: DOPAC/1:5), at the final concentrations of 5 μM (monomer concentration). (A) Representative confocal scanning microscopy images of SH-SY5Y cells exposed to different aggregates for 24 h. The cell membranes were stained with Alexa 488-conjugated CTX-B (green fluorescence); the cell nuclei with Hoechst 33342 (blue fluorescence), and the protein aggregates with anti-Syn antibodies followed by treatment with Alexa 568-conjugated anti rabbit secondary antibodies (red fluorescence). Protein colocalization with GM1 (top panels). Scale bars are 14 μm in all images. FRET efficiency is shown in the bottom panels. (B) Representative confocal microscopy images of Fluo3-AM loaded SH-SY5Y cells exposed for 2 h to 5 μM different aggregates. The cells were grown in complete (left) or in calcium-free (right) medium. In each column representative differential interference contrast (DIC) images (right) and intracellular free Ca^{2+} fluorescence signal images (left) are shown. Scale bars are 18.5 μm in all images. (C) Representative kinetic traces of SH-SY5Y cells loaded with Fluo-3 AM, treated with different aggregates and monitored for 2 h. The cells were grown in complete medium (top panel) or in free Ca^{2+} medium (bottom panel). Fluo-3 AM-treated cells were used as a control (black line); after addition of Syn aggregates (orange) and Syn/DOPAC aggregates (yellow); after addition of E46K aggregates (dark green) and E46K/DOPAC aggregates (light green). (D, E) Mitochondrial activities were analyzed in terms of MTT reduction (D) and ROS production (E) detected by CH_2-DCFDA probe. Values refer to 4 (black column) and 24 (grey column) h of incubation with different aggregates. Data were reported as the mean of three independent experiments performed in triplicates ± SE. Statistical analysis: $^{**}p < 0.01$; $^{***}p < 0.001$ vs untreated cells (CTRL). $^{\circ}p < 0.05$: $^{\circ\circ}$ $p < 0.01$; $^{\circ\circ\circ}$ $p < 0.001$ vs E46K and Syn alone.

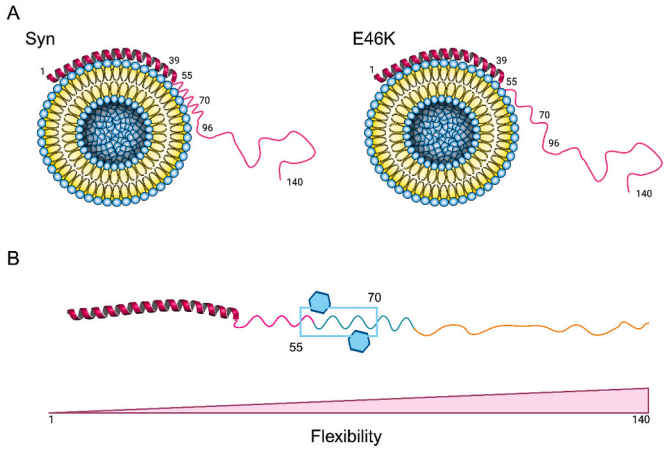

Scheme 1. Comparison between the modality of interaction of Syn and E46K with SUV. Both proteins show the N-terminal helical domain (residues 1–55) anchored to the membrane and different flexibility at the level of the 55–90 region: in Syn results to be more rigid, while it is dynamically available for other interaction in E46K (A). Proposed site of DOPAC binding to protein. The pink region represents the N-terminal helical segment interacting with the membrane, while the blue and orange lines illustrate different flexibility zones. The blue box refers to the proposed DOPAC binding sites, confined in the 55–70 region. The plot below emphasizes the protein increasing flexibility from residue 1 to 140, with significant changes in regions of membrane interaction.

resembles that previously proposed one probed by NMR techniques in the limits determined by technical timescale [6,23] (Scheme 1). The N-terminal segment is firmly bound to the membrane, the central region interacts dynamically, and the C-terminal region (96–140) is disordered and free in the cytosol. In the model proposed by Fusco et al., the first 25 residues, called membrane anchor region, are strongly engaged with the vesicles, while the amino acid stretch 26–97, defined membrane sensor region, transiently binds the membrane. Taking the deuterium exchange value as an index of the protein flexibility and mobility, under our experimental conditions, the anchor region extends to residue 39 in Syn, shortening the sensor region to 40–95 stretch. The C-terminal tail persists in solution as a disordered and flexible region as seen in all models of Syn/lipid interaction [50]. The reduced temporal resolution of HDX techniques compared to HR-NMR may be insufficient to discriminate which regions interact more strongly in fast equilibria, however it allowed us to capture valuable insights regarding the overall strong interaction within the entire segment. By HDX-MS analysis, the 18–39 region shows very low deuterium incorporation (10 %) in both proteins and the residues from 95 onwards reach a percentage close to 100 %, as expected. The most significant difference between Syn and E46K upon binding to membrane was observed in the 40–95 region, where a gradual increase in the exchange percentage can be detected along the sequence reaching 30 % in Syn and 50 % in E46K. The wider deuterium incorporation in E46K in the entire extent of the 40–95 region is thus consistent with greater mobility and dynamics in the mutant in comparison to Syn. This higher conformational flexibility of the mutant matches the results obtained by SPR, allowing us to conclude that E46K is characterized by greater mobility when bound to SUV than Syn. When free in solution, the two molecules exhibited different behavior resulting E46K more compact than Syn [26]. Therefore, the longer time taken by E46K to acquire secondary structure in contact with membranes could be the result of two distinct events: the interruption of the long-range stabilizing interactions and the short-life of the stable bound conformation characterized by a fast bound-unbound equilibrium.

When the complexes P/DOPAC are mixed with SUV (P/DOPAC + SUV), they stably bind to vesicles through the region 1–39, as do the proteins alone. The remnant of the lipid-binding domain of the two proteins behaves differently. DOPAC affects the deuterium exchange of 55–70 region of Syn, in the protein/SUV system, accounting for an increase of 10 % (from 30 to 40 %). In contrast, it has no effect on the mutant. Indeed, the region 55–70 in E46K/DOPAC appears still transiently exposed upon lipid-induced folding like in the absence of the catechol. Therefore, our previous hypothesis that DOPAC preferentially recognizes the segment 55–70 is likely to be further supported [25,26,51]. Of note, CD measurements detected a reduced content of α-helical secondary structure upon membrane binding for both proteins, even more for E46K, after their incubation with DOPAC for 48 h. At this stage, stable catechol-induced off-pathway oligomers constitute the main conformational population [25,26]. Therefore, the 55–70 stretch in the oligomeric protein is hidden by the interaction with DOPAC or as the result of the incubation in the presence of DOPAC, preventing the possibility for the proteins to further interact with SUV. The different membrane affinity of DOPAC-modified aggregates compared to unmodified aggregates was also evaluated in cultured human neuroblastoma cells, SH-SY5Y. Indeed, DOPAC-modified aggregates showed reduced FRET efficiency with GM1 on the SH-SY5Y cell membrane, reduced membrane destabilization, as indicated by calcium flux measurements, as well as reduced cytotoxicity and reactive oxygen species (ROS) production compared to unmodified aggregates. This suggests that DOPAC modification may confer protective effects against the toxic effects of Syn on neuronal membranes.

On the other hand, analyzing the action of DOPAC on the protein/membrane system in saturation conditions (P/SUV + DOPAC), the catechol seems to affect only the mutant, increasing its ability to exchange hydrogens in the 55–70 region, where an exchange of 70 % is detected upon DOPAC addition. This further confirms that this amino acid region is more mobile in E46K and is exposed to the solvent long enough for DOPAC to bind. In Syn, it remains more firmly anchored to the membranes and does not expose the conformational space required for DOPAC to bind (Scheme 2). Prolonging the incubation (48 h) with DOPAC in quiescence conditions (no possible aggregation event), the catechol further competes with the binding of the protein with SUV inducing E46K displacement, with no effect on Syn, as shown by CD

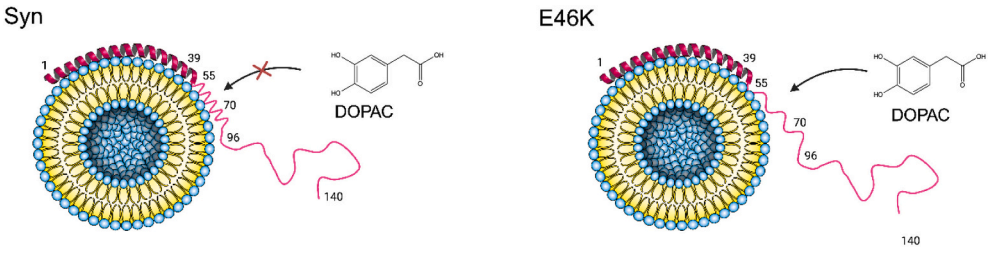

Scheme 2. Protein displacement by DOPAC. The scheme shows the differences in the interaction model of the two proteins with SUVs. The 55–90 amino acid region in Syn is firmly anchored to the membranes, while it appears more mobile in E46K. Therefore, the proposed binding region for DOPAC (residues 55–70) seems more rigid and thus less available in Syn than E46K. Hence, the conformational space required for DOPAC to bind is exposed in E46K and not in Syn.

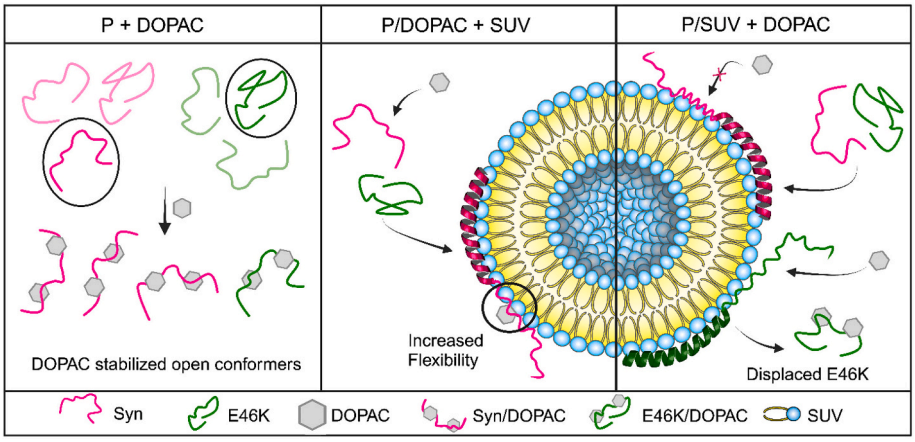

Summarizing scheme. DOPAC effect on Syn and E46K dynamics in solution (left panel) and upon interaction with membranes (center and right panels). In the conformational ensemble populated by Syn and E46K, Syn adopts a more extended and E46K a more compact state (circled). DOPAC selects and stabilizes their extended conformations (left). P/DOPAC complexes retain their ability to bind SUVs. Notably, Syn/DOPAC exhibits an increase in mobility in the region 40–95 (circled), compared to the protein alone bound to SUV (center). When bound to SUV, E46K exhibits higher mobility in the 40–95 region compared to Syn. Indeed, DOPAC seems to affect only E46K increasing its mobility in the region 55–70, therefore suggesting that this region in E46K is dynamically exposed for a sufficient time to allow DOPAC to bind (right).

measurements. The same experiment was conducted by using a protein/lipid ratio leaving 50 % of protein molecules in the free form. In this case, DOPAC could interact with both populations of the protein, the bound and the unbound ones. Since its faster bound-unbound equilibrium, as previously observed, E46K binding is affected by DOPAC immediately and even more upon 48 h-incubation in quiescence. Vice versa, as expected, the catechol fails in the displacement of the bound form of Syn. Therefore, we can conclude that DOPAC exhibits a preference for the membrane-bound species of E46K. Of note, E46K, while in solution populates preferentially a compact conformation [22,26,43], upon binding to SUV, it exhibits a relaxed region exposed to solvent. Conversely, the more extended conformation of Syn in solution fairly interacts with DOPAC, more than the rigid lipid-bound species. This is corroborated by the observation that upon further addition of DOPAC molecules to the system constituted by the protein/SUV incubated for 48 h, E46K undergoes displacement following the addition of the catechol in higher extent than Syn. For both proteins, adding new protein molecules restore the α-helical secondary structure content of the proteins bound to SUV after 48 h (cfr Fig. 8B_1, D_1). Of note, if the system already contains DOPAC (P/SUV + DOPAC +48 h), a further addition of the catechol has a slight effect in the case of Syn and a robust one for E46K, while a further addition of protein allows the complete acquisition of the initial secondary structure in Syn but not in E46K (cfr Fig. 8B_2, D_2).

In conclusion, the approaches used, mainly based on biophysical measurements, provided a suitable method to study a dynamic process highlighting and confirming substantial differences between Syn and its pathological mutant E46K (Summarizing scheme). Even if in a not-quantitative way, a catechol-containing compound demonstrated its ability to partially compete with Syn for membrane binding by using the same concentration efficacious for the inhibition of the protein aggregation in solution. Finally, DOPAC is a dopamine metabolite that could be actively involved in the modulation of Syn levels within the neuronal environment when the protein is in free or bound form. These possible roles of DOPAC highlight the need for further research into its mechanisms and potential therapeutic implications, particularly regarding neurodegenerative diseases in which dopamine dysregulation is a hallmark such as in PD. The beneficial effect of this small molecule must be put into perspective to convert it into therapeutics, that is a major challenge and to overcome the bioavailability limitation of this type of compounds a real strategy could be represented only by tailored nanomedicine [52].

CRediT authorship contribution statement

Elena Rizzotto: Investigation, Formal analysis, Data curation, Conceptualization. **Andrea Pierangelini:** Investigation, Formal analysis, Data curation, Conceptualization. **Benedetta Fongaro:** Writing – review & editing, Validation, Investigation, Formal analysis. **Manuela Leri:** Investigation, Formal analysis, Data curation. **Ilenia Inciardi:** Formal analysis. **Philipp Trolese:** Writing – review & editing, Formal analysis. **Vincenzo De Filippis:** Writing – review & editing. **Monica Bucciantini:** Writing – review & editing, Writing – original draft, Investigation. **Laura Acquasaliente:** Writing – review & editing, Writing – original draft, Formal analysis. **Patrizia Polverino de Laureto:** Writing – review & editing, Writing – original draft, Project administration, Funding acquisition.

Funding

This project was supported by a competitive grant from University of Padova (Progetti di Ateneo, 2022, BIRD222840), which has also financed I.I. ML was supported by Fondazione Veronesi.

Declaration of competing interest

The authors declare that they have no known competing financial interests or personal relationships that could have appeared to influence the work reported in this paper.

Appendix A. Supplementary data

Supplementary data to this article can be found online at https://doi.org/10.1016/j.ijbiomac.2024.139427.

References

[1] W. Poewe, K. Seppi, C.M. Tanner, G.M. Halliday, P. Brundin, J. Volkmann, A.-E. Schrag, A.E. Lang, Parkinson disease, Nat. Rev. Dis. Prim. 3 (1) (2017) 1–21, https://doi.org/10.1038/nrdp.2017.13.
[2] M.G. Spillantini, M.L. Schmidt, V.M.-Y. Lee, J.Q. Trojanowski, R. Jakes, M. Goedert, α-Synuclein in Lewy Bodies, Nature 388 (6645) (1997) 839–840, https://doi.org/10.1038/42166.
[3] P.H. Weinreb, W. Zhen, A.W. Poon, K.A. Conway, P.T. Lansbury, NACP, a protein implicated in Alzheimer's disease and learning, is natively unfolded, Biochemistry 35 (43) (1996) 13709–13715, https://doi.org/10.1021/bi961799n.
[4] C.W. Bertoncini, Y.-S. Jung, C.O. Fernandez, W. Hoyer, C. Griesinger, T.M. Jovin, M. Zweckstetter, Release of long-range tertiary interactions potentiates aggregation

of natively unstructured α-Synuclein, Proc. Natl. Acad. Sci. 102 (5) (2005) 1430–1435, https://doi.org/10.1073/pnas.0407146102.
[5] W.S. Davidson, A. Jonas, D.F. Clayton, J.M. George, Stabilization of α-Synuclein secondary structure upon binding to synthetic membranes *, J. Biol. Chem. 273 (16) (1998) 9443–9449, https://doi.org/10.1074/jbc.273.16.9443.
[6] G. Fusco, A. De Simone, T. Gopinath, V. Vostrikov, M. Vendruscolo, C.M. Dobson, G. Veglia, Direct observation of the three regions in α-Synuclein that determine its membrane-bound behaviour, Nat. Commun. 5 (1) (2014) 3827, https://doi.org/10.1038/ncomms4827.
[7] G. De Franceschi, E. Frare, L. Bubacco, S. Mammi, A. Fontana, P.P. de Laureto, Molecular insights into the interaction between α-Synuclein and docosahexaenoic acid, J. Mol. Biol. 394 (1) (2009) 94–107, https://doi.org/10.1016/j.jmb.2009.09.008.
[8] K. Uéda, H. Fukushima, E. Masliah, Y. Xia, A. Iwai, M. Yoshimoto, D.A. Otero, J. Kondo, Y. Ihara, T. Saitoh, Molecular cloning of cDNA encoding an unrecognized component of amyloid in Alzheimer disease, Proc. Natl. Acad. Sci. 90 (23) (1993) 11282–11286, https://doi.org/10.1073/pnas.90.23.11282.
[9] P.P. de Laureto, L. Tosatto, E. Frare, O. Marin, V.N. Uversky, A. Fontana, Conformational properties of the SDS-bound state of α-Synuclein probed by limited proteolysis: unexpected rigidity of the acidic C-terminal tail, Biochemistry 45 (38) (2006) 11523–11531, https://doi.org/10.1021/bi052614s.
[10] W. Hoyer, D. Cherny, V. Subramaniam, T.M. Jovin, Impact of the acidic C-terminal region comprising amino acids 109−140 on α-Synuclein aggregation in vitro, Biochemistry 43 (51) (2004) 16233–16242, https://doi.org/10.1021/bi048453u.
[11] D.F. Clayton, J.M. George, The Synucleins: a family of proteins involved in synaptic function, plasticity, neurodegeneration and disease, Trends Neurosci. 21 (6) (1998) 249–254, https://doi.org/10.1016/S0166-2236(97)01213-7.
[12] J. Burré, The synaptic function of α-Synuclein, J. Parkinsons Dis. 5 (4) (2015) 699–713, https://doi.org/10.3233/JPD-150642.
[13] J.Q. Trojanowski, V.M.-Y. Lee, Parkinson's disease and related α-Synucleinopathies are brain Amyloidoses, Ann. N. Y. Acad. Sci. 991 (1) (2003) 107–110, https://doi.org/10.1111/j.1749-6632.2003.tb07468.x.
[14] B. Winner, R. Jappelli, S.K. Maji, P.A. Desplats, L. Boyer, S. Aigner, C. Hetzer, T. Loher, M. Vilar, S. Campioni, C. Tzitzilonis, A. Soragni, S. Jessberger, H. Mira, A. Consiglio, E. Pham, E. Masliah, F.H. Gage, R. Riek, In vivo demonstration that α-Synuclein oligomers are toxic, Proc. Natl. Acad. Sci. 108 (10) (2011) 4194–4199, https://doi.org/10.1073/pnas.1100976108.
[15] G.A.P. de Oliveira, J.L. Silva, Alpha-Synuclein stepwise aggregation reveals features of an early onset mutation in Parkinson's disease, Commun. Biol. 2 (1) (2019) 1–13, https://doi.org/10.1038/s42003-019-0598-9.
[16] P. Flagmeier, G. Meisl, M. Vendruscolo, T.P.J. Knowles, C.M. Dobson, A.K. Buell, C. Galvagnion, Mutations associated with familial Parkinson's disease alter the initiation and amplification steps of α-Synuclein aggregation, Proc. Natl. Acad. Sci. 113 (37) (2016) 10328–10333, https://doi.org/10.1073/pnas.1604645113.
[17] I. Íñigo-Marco, M. Valencia, L. Larrea, R. Bugallo, M. Martínez-Goikoetxea, I. Zuriguel, M. Arrasate, E46K α-Synuclein pathological mutation causes cell-autonomous toxicity without altering protein turnover or aggregation, Proc. Natl. Acad. Sci. 114 (39) (2017) E8274–E8283, https://doi.org/10.1073/pnas.1703420114.
[18] J.J. Zarranz, J. Alegre, J.C. Gómez-Esteban, E. Lezcano, R. Ros, I. Ampuero, L. Vidal, J. Hoenicka, O. Rodriguez, B. Atarés, V. Llorens, E.G. Tortosa, T. del Ser, D.G. Muñoz, J.G. de Yebenes, The new mutation, E46K, of α-Synuclein causes Parkinson and Lewy body dementia, Ann. Neurol. 55 (2) (2004) 164–173, https://doi.org/10.1002/ana.10795.
[19] O. Wise-Scira, A. Dunn, A.K. Aloglu, I.T. Sakallioglu, O. Coskuner, Structures of the E46K mutant-type α-Synuclein protein and impact of E46K mutation on the structures of the wild-type α-Synuclein protein, ACS Chem. Neurosci. 4 (3) (2013) 498–508, https://doi.org/10.1021/cn3002027.
[20] C.C. Rospigliosi, S. McClendon, A.W. Schmid, T.F. Ramlall, P. Barré, H.A. Lashuel, D. Eliezer, E46K Parkinson's-linked mutation enhances C-terminal-to-N-terminal contacts in α-Synuclein, J. Mol. Biol. 388 (5) (2009) 1022–1032, https://doi.org/10.1016/j.jmb.2009.03.065.
[21] G. Fusco, T. Pape, A.D. Stephens, P. Mahou, A.R. Costa, C.F. Kaminski, G. S. Kaminski Schierle, M. Vendruscolo, G. Veglia, C.M. Dobson, A. De Simone, Structural basis of synaptic vesicle assembly promoted by α-Synuclein, Nat. Commun. 7 (1) (2016) 12563, https://doi.org/10.1038/ncomms12563.
[22] M. Rovere, A.E. Powers, H. Jiang, J.C. Pitino, L. Fonseca-Ornelas, D.S. Patel, A. Achille, R. Langen, J. Varkey, T. Bartels, E46K-like α-Synuclein mutants increase lipid interactions and disrupt membrane selectivity, J. Biol. Chem. 294 (25) (2019) 9799–9812, https://doi.org/10.1074/jbc.RA118.006551.
[23] C.R. Bodner, A.S. Maltsev, C.M. Dobson, A. Bax, Differential phospholipid binding of α-Synuclein variants implicated in Parkinson's disease revealed by solution NMR spectroscopy, Biochemistry 49 (5) (2010) 862–871, https://doi.org/10.1021/bi901723p.
[24] L. Palazzi, E. Bruzzone, G. Bisello, M. Leri, M. Stefani, M. Bucciantini, P. Polverino de Laureto, Oleuropein aglycone stabilizes the monomeric α-Synuclein and favours the growth of non-toxic aggregates, Sci. Rep. 8 (1) (2018) 8337, https://doi.org/10.1038/s41598-018-26645-5.
[25] L. Palazzi, B. Fongaro, M. Leri, L. Acquasaliente, M. Stefani, M. Bucciantini, P. Polverino de Laureto, Structural features and toxicity of α-Synuclein oligomers grown in the presence of DOPAC, Int. J. Mol. Sci. 22 (11) (2021) 6008, https://doi.org/10.3390/ijms22116008.
[26] B. Fongaro, E. Cappelletto, A. Sosic, B. Spolaore, P. Polverino de Laureto, 3,4-Dihydroxyphenylethanol and 3,4-Dihydroxyphenylacetic acid affect the aggregation process of E46K variant of α-Synuclein at different extent: insights into the interplay between protein dynamics and catechol effect, Protein Sci. 31 (7), e4356 (2022), https://doi.org/10.1002/pro.4356.
[27] J. Meiser, D. Weindl, K. Hiller, Complexity of dopamine metabolism, Cell Commun. Signal 11 (1) (2013) 34, https://doi.org/10.1186/1478-811X-11-34.
[28] M.O. Klein, D.S. Battagello, A.R. Cardoso, D.N. Hauser, J.C. Bittencourt, R. G. Correa, Dopamine: functions, signaling, and association with neurological diseases, Cell. Mol. Neurobiol. 39 (1) (2019) 31–59, https://doi.org/10.1007/s10571-018-0632-3.
[29] F. Stocchi, D. Bravi, A. Emmi, A. Antonini, Parkinson disease therapy: current strategies and future research priorities, Nat. Rev. Neurol. 20 (12) (2024) 695–707, https://doi.org/10.1038/s41582-024-01034-x.
[30] A. Zafra-Gómez, B. Luzón-Toro, S. Capel-Cuevas, J.C. Morales, Stability of Hydroxytyrosol in aqueous solutions at different concentration, temperature and with different ionic content: a study using UPLC-MS, Food Nutr. Sci. 2 (10) (2011) 1114–1120, https://doi.org/10.4236/fns.2011.210149.
[31] B. Mui, L. Chow, M.J. Hope, Extrusion technique to generate liposomes of defined size, in: *Methods in Enzymology*; Liposomes, Part A vol. 367, Academic Press, 2003, pp. 3–14, https://doi.org/10.1016/S0076-6879(03)67001-1.
[32] S.C. Gill, P.H. von Hippel, Calculation of protein extinction coefficients from amino acid sequence data, Anal. Biochem. 182 (2) (1989) 319–326, https://doi.org/10.1016/0003-2697(89)90602-7.
[33] L. Konermann, J. Pan, Y.-H. Liu, Hydrogen exchange mass spectrometry for studying protein structure and dynamics, Chem. Soc. Rev. 40 (3) (2011) 1224–1234, https://doi.org/10.1039/C0CS00113A.
[34] D. Peterle, T.E. Wales, J.R. Engen, Simple and fast Maximally Deuterated Control (maxD) preparation for hydrogen–deuterium exchange mass spectrometry experiments, Anal. Chem. 94 (28) (2022) 10142–10150, https://doi.org/10.1021/acs.analchem.2c01446.
[35] D. Nosi, R. Mercatelli, F. Chellini, S. Soria, A. Pini, L. Formigli, F. Quercioli, A molecular imaging analysis of Cx43 association with Cdo during skeletal myoblast differentiation, J. Biophotonics 6 (8) (2013) 612–621, https://doi.org/10.1002/jbio.201200063.
[36] W.K. Man, B. Tahirbegi, M.D. Vrettas, S. Preet, L. Ying, M. Vendruscolo, A. De Simone, G. Fusco, The docking of synaptic vesicles on the presynaptic membrane induced by α-Synuclein is modulated by lipid composition, Nat. Commun. 12 (1) (2021) 927, https://doi.org/10.1038/s41467-021-21027-4.
[37] M. Kiechle, V. Grozdanov, K.M. Danzer, The role of lipids in the initiation of α-Synuclein misfolding, Front. Cell Dev. Biol. (2020) 8, https://doi.org/10.3389/fcell.2020.562241.
[38] C. Galvagnion, A.K. Buell, G. Meisl, T.C.T. Michaels, M. Vendruscolo, T.P. J. Knowles, C.M. Dobson, Lipid vesicles trigger α-Synuclein aggregation by stimulating primary nucleation, Nat. Chem. Biol. 11 (3) (2015) 229–234, https://doi.org/10.1038/nchembio.1750.
[39] A.S. Maltsev, J. Chen, R.L. Levine, A. Bax, Site-specific interaction between α-Synuclein and membranes probed by NMR-observed methionine oxidation rates, J. Am. Chem. Soc. 135 (8) (2013) 2943–2946, https://doi.org/10.1021/ja312415q.
[40] A. Camilleri, C. Zarb, M. Caruana, U. Ostermeier, S. Ghio, T. Högen, F. Schmidt, A. Giese, N. Vassallo, Mitochondrial membrane permeabilisation by amyloid aggregates and protection by polyphenols, Biochim. Biophys. Acta Biomembr. 1828 (11) (2013) 2532–2543, https://doi.org/10.1016/j.bbamem.2013.06.026.
[41] M. Gonzalez-Garcia, G. Fusco, A. De Simone, Membrane interactions and toxicity by misfolded protein oligomers, Front. Cell Dev. Biol. (2021) 9, https://doi.org/10.3389/fcell.2021.642623.
[42] J. Parres-Gold, A. Chieng, S. Wong Su, Y. Wang, Real-time characterization of cell membrane disruption by α-Synuclein oligomers in live SH-SY5Y neuroblastoma cells, ACS Chem. Neurosci. 11 (17) (2020) 2528–2534, https://doi.org/10.1021/acschemneuro.0c00309.
[43] D.R. Boyer, B. Li, C. Sun, W. Fan, K. Zhou, M.P. Hughes, M.R. Sawaya, L. Jiang, D. S. Eisenberg, The α-Synuclein hereditary mutation E46K unlocks a more stable, pathogenic fibril structure, Proc. Natl. Acad. Sci. USA 117 (7) (2020) 3592–3602, https://doi.org/10.1073/pnas.1917914117.
[44] P.K. Auluck, G. Caraveo, S. Lindquist, α-Synuclein: membrane interactions and toxicity in Parkinson's disease, Annu. Rev. Cell Dev. Biol. 26 (2010) 211–233, https://doi.org/10.1146/annurev.cellbio.042308.113313.
[45] V.V. Shvadchak, L.J. Falomir-Lockhart, D.A. Yushchenko, T.M. Jovin, Specificity and kinetics of α-Synuclein binding to model membranes determined with fluorescent Excited State Intramolecular Proton Transfer (ESIPT) probe *, J. Biol. Chem. 286 (15) (2011) 13023–13032, https://doi.org/10.1074/jbc.M110.204776.
[46] S.H. Shahmoradian, A.J. Lewis, C. Genoud, J. Hench, T.E. Moors, P.P. Navarro, D. Castaño-Díez, G. Schweighauser, A. Graff-Meyer, K.N. Goldie, R. Sütterlin, E. Huisman, A. Ingrassia, Y. de Gier, A.J.M. Rozemuller, J. Wang, A.D. Paepe, J. Erny, A. Staempfli, J. Hoernschemeyer, F. Großerüschkamp, D. Niedieker, S. F. El-Mashtoly, M. Quadri, W.F.J. Van IJcken, V. Bonifati, K. Gerwert, B. Bohrmann, S. Frank, M. Britschgi, H. Stahlberg, W.D.J. Van de Berg, M.E. Lauer, Lewy pathology in Parkinson's disease consists of crowded organelles and lipid membranes, Nat. Neurosci. 22 (7) (2019) 1099–1109, https://doi.org/10.1038/s41593-019-0423-2.

[47] K. Makasewicz, S. Wennmalm, B. Stenqvist, M. Fornasier, A. Andersson, P. Jönsson, S. Linse, E. Sparr, Cooperativity of α-Synuclein binding to lipid membranes, ACS Chem. Neurosci. 12 (12) (2021) 2099–2109, https://doi.org/10.1021/acschemneuro.1c00006.

[48] D.P. Smith, D.J. Tew, A.F. Hill, S.P. Bottomley, C.L. Masters, K.J. Barnham, R. Cappai, Formation of a high affinity lipid-binding intermediate during the early aggregation phase of α-Synuclein, Biochemistry 47 (5) (2008) 1425–1434, https://doi.org/10.1021/bi701522m.

[49] K. Pirc, V. Hodnik, N. Poklar Ulrih, G. Anderluh, Interaction of α-Synuclein with negatively charged lipid membranes monitored by surface Plasmon resonance, Croat. Chem. Acta 89 (2) (2016) 255–260, https://doi.org/10.5562/cca2889.

[50] I. Dikiy, D. Eliezer, Folding and Misfolding of alpha-Synuclein on membranes, Biochim. Biophys. Acta 1818 (4) (2012) 1013–1018, https://doi.org/10.1016/j.bbamem.2011.09.008.

[51] Inciardi, I.; Rizzotto, E.; Gregoris, F.; Fongaro, B.; Sosic, A.; Minervini, G.; Polverino de Laureto, P. Catechol-induced covalent modifications modulate the aggregation tendency of α-Synuclein: an in-solution and in-silico study. BioFactors n/a (n/a). doi:https://doi.org/10.1002/biof.2086.

[52] J.J. Mulvihill, E.M. Cunnane, A.M. Ross, J.T. Duskey, G. Tosi, A.M. Grabrucker, Drug delivery across the blood–brain barrier: recent advances in the use of nanocarriers, Nanomed 15 (2) (2020) 205–214, https://doi.org/10.2217/nnm-2019-0367.